photonics

MDPI

Communication

74.7% Efficient GaAs-Based Laser Power Converters at 808 nm at 150 K

Simon Fafard * and Denis P. Masson

Broadcom (Canada), IFPD, Ottawa, ON K1A 0R6, Canada
* Correspondence: simon.fafard@broadcom.com

Abstract: High-efficiency multijunction laser power converters are demonstrated for low temperature applications with an optical input at 808 nm. The photovoltaic power converting III-V semiconductor devices are designed with GaAs absorbing layers, here with 5 thin subcells (PT5), connected by transparent tunnel junctions. Unprecedented conversion efficiencies of up to 74.7% are measured at temperatures around 150 K. At temperatures around 77 K, a remarkably low bandgap offset value of W_{oc} = 71 mV is obtained at an optical input intensity of ~7 W/cm^2. At 77 K, the PT5 retains an efficiency of 65% with up to 0.3 W of converted output power.

Keywords: optical power converters; laser power converters; power-over-fiber; power beaming; photovoltaic; galvanic isolation; GaAs; multijunctions semiconductor heterostructures; cryogenic temperatures; bandgap offset (W_{oc})

1. Introduction

Impressive laser Optical Power Converters (OPCs) results have been obtained for various wavelength ranges and output power capabilities [1–47]. Our recent Power Converter Performance Chart [41,47] clearly highlights that multijunction OPCs are most advantageous to obtain high device performance. The research related to photovoltaic devices also suggests other potential future device improvements [48–67], as well as new optical wireless power transmission (OWPT) applications and design strategies for future systems [68–78].

In typical cases, the OPC devices are expected to operate near room temperature, or more generally to function efficiently in a range between −40 °C and 85 °C. However, space applications or scientific experiments requiring cryogenic temperatures [79] could benefit from OPC devices capable of high-performance at temperatures as low as 77 K.

From the laser diode perspective, many of the OPC developments have historically been achieved at wavelengths around 808 nm due to the ubiquity and the maturity of GaAs-based lasers at this wavelength. An input wavelength at 808 nm will actually be close to optimal for OPCs designed with GaAs absorbing layers as the band-edge shifts to a wavelength of 822 nm at 77 K. Indeed, having the optical input wavelength only at ~14 nm (~26 meV) above the edge of the semiconductor bandgap is advantageous for minimizing the photocarrier thermalization losses and for optimizing the OPC's efficiency.

In this study, we therefore measure the characteristics of vertical multijunction OPCs with 5 thin GaAs subcells (PT5) at cryogenic temperatures, with an input wavelength at 808 nm. The temperature dependence of the key OPC parameters is measured for a PT5 based on the Vertical Epitaxial Heterostructure Architecture (VEHSA) design [57]. This study focuses on a PT5 design which was originally intended for operating near room temperature at a input wavelength of near 850 nm. This design is also expected to be near ideal at low temperatures due to the GaAs bandgap shift combined with the swap of the optical input from 850 nm to 808 nm.

check for updates

Citation: Fafard, S.; Masson, D.P. 74.7% Efficient GaAs-Based Laser Power Converters at 808 nm at 150 K. *Photonics* **2022**, *9*, 579. https://doi.org/10.3390/photonics9080579

Received: 21 July 2022
Accepted: 16 August 2022
Published: 17 August 2022

Publisher's Note: MDPI stays neutral with regard to jurisdictional claims in published maps and institutional affiliations.

2. Materials and Methods

The schematic of the PT5 heterostructure is depicted in Figure 1a. It is based on the previously described VEHSA design [57,58]. The Beer-Lambert law was used to calculate the individual subcell's absorber thicknesses, here with each subcell absorbing ~ 1/5 of the incident light. Specifically, the thicknesses for the GaAs absorber subcells used here were 192, 246, 346, 581, and 2636 nm, from top to bottom, respectively. It should be noted that methods have now also been put forward based on machine learning and genetic algorithm for improving the optimization of the individual thicknesses [80]. Such a model suggests for example that the evaluation using the Beer-Lambert model might be underestimating the required thickness of the first subcell.

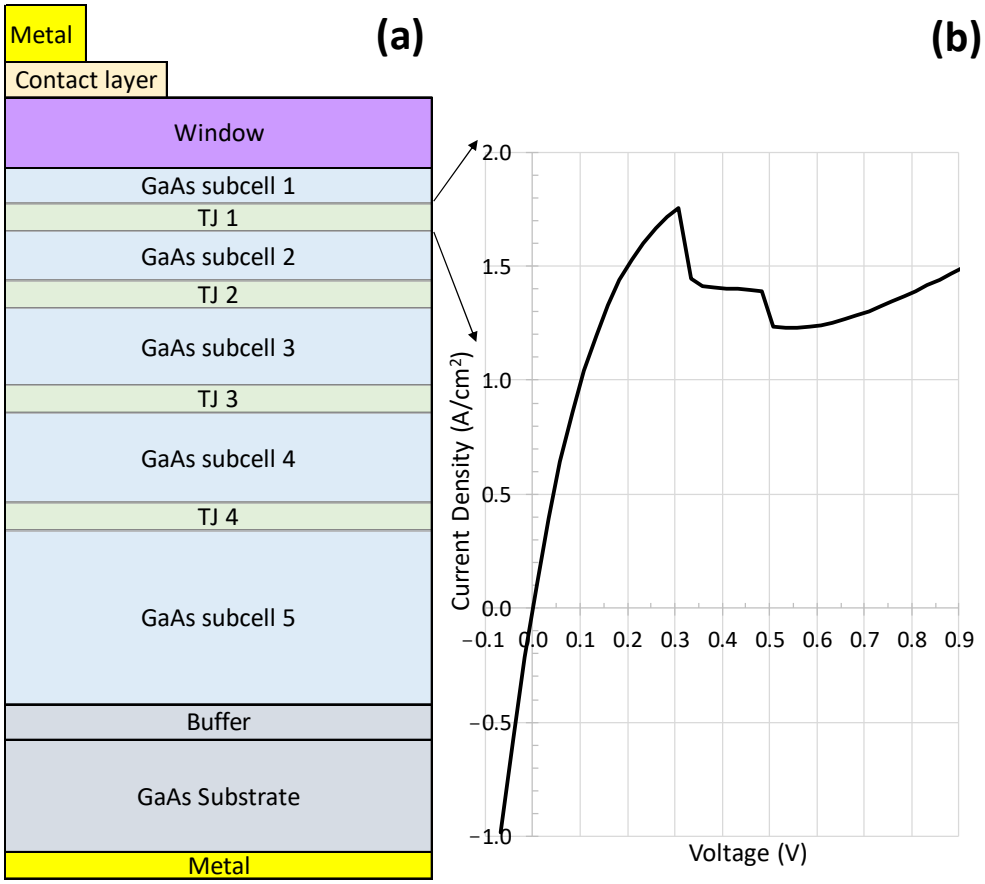

Figure 1. Schematic of the PT5 Vertical Epitaxial HeteroStructure Architecture (VEHSA design) devices prepared with 5 GaAs subcells in (**a**), and average current density vs voltage characteristic of a tunnel junction (TJ) measured from the PT5 structure when the incident optical intensity was high enough to trigger the first TJ negative differential resistance (NDR) behavior in (**b**).

The photovoltaic vertical multijunction structure was built for operation at T ~ 20 °C with the optical input from a laser source emitting in a spectral range peaking around 850 nm. The predominant change in the GaAs absorption coefficient between 20 °C and 77 K is a shift towards shorter wavelengths. Therefore, we expect the same design will be near-optimal for an optical input wavelength of 808 nm at cryogenic temperatures. The PT5 is designed with 5 optically transparent photovoltaic semiconductor subcells interconnected with tunnel junctions, labelled TJi in Figure 1a. Each individual subcell comprises an n-type emitter and a p-type base. The TJs are made to be transparent to the input beam, utilizing AlGaAs-AlInGaP alloys lattice-matched to GaAs.

The underlying TJ's current-voltage (I-V) characteristics can be deduced from PT5 I-V characteristics taken under optical input intensities that are exceeding the TJ's peak current capability. For example, Figure 1b shows the PT5 I-V curve rescaled to distinguish the TJ

characteristic more clearly. The horizontal axis plots Voc—V, whereas the vertical axis is inverted compared to the plot of a typical p/n junction I-V curve. This approach reveals the negative differential resistance (NRD) region of one of the TJs (NDR observed for 0.3 V < V < 0.9 V), thus confirming the tunnel current characteristics at 77 K. As previously observed when the NDR arises, the illuminated I-V is discontinuous for that region. This particular PT5 structure had a peak tunneling current capabilities of the order of A/cm^2, but we are confident that designs with significantly higher peak current capability are readily achievable [57].

The epitaxial layers are grown using commercial production Aixtron Metal Organic Chemical Vapor Deposition (MOCVD) reactors. The total thickness of all the emitter and base layers from the different subcells is such that the impinging optical beam is almost completely absorbed for the condition of 850 nm at 20 °C, or similarly for 808 nm at 77 K. As described previously [41,58], to realize the required photocurrent matching condition, the structure usually has increasing subcell thicknesses from the top subcell (thinnest) toward the bottom subcell (thickest). Furthermore, the vertical multijunction devices can also benefit from strong photon coupling and recycling within, and between, the constituent subcells [81–84]. Potentially the photon coupling and recycling effects could be even more significant at low temperatures, in which case the radiative recombination is typically prominent.

The PT5 wafers were fabricated into chips with an area of 0.03 cm^2. The device fabrication included standard blanket back-metallization, front ohmic contacts, and antireflection coatings (ARC) constructed from layers of Al_2O_3 and TiO_2. The ARC typically reduces the reflectivity (R) of the incident beam to R < 4% for the spectral range of interest.

A 808 nm fiber-coupled laser diode manufactured by BWT was used [85]. It had a numerical aperture of NA ~0.22, using a multi-mode fiber core diameter of 400 μm and cladding of 440 μm. The PT5 devices were packaged in Broadcom's *regular power* housing equipped with an FC optical connector [37]. The I-V characteristics were acquired using a Keithley 2601B source-meter. For most of the I-V measurements, the fiber-coupled laser was connected to the packaged PT5 using an FC connector. The FC connection was further sealed using a Kapton tape and the device was immersed in liquid nitrogen for the 77 K measurements. For variable temperature measurements, either the device was let to warm up after the liquid nitrogen was all evaporated, or a liquid nitrogen cryostat was used equipped with a standard 1 kOhms resistive temperature device (RTD) to directly measure the device temperature. Quick I-V scans were used to avoid significant chip heating or temperature drifts between the measurements.

3. Results

The PT5 characteristics at 77 K are shown in Figure 2. The measured I-V curves are shown in Figure 2a for various optical input powers between P_{in} = 96 mW and P_{in} = 372 mW. The dashed (pink) curve of Figure 2a is an ideal diode model fitted to the 96 mW data. A good fit is obtained, here using 5 diodes all with the same ideality factor of n = 1.6 and a quantum efficiency of EQE = 79%. The fitted photocurrent ratios for the 5 subcells (from bottom to top) are respectively 100%, 99%, 98%, 97%, and 96%. The fit reproduces well the data when the overall series resistance is set to be smaller than ~0.1 Ohm.

Figure 2b shows that the output power P_{mpp} has a measured slope efficiency of Eff ~65% at 77 K, with negligible deviations from a linear regression for optical input powers up to ~0.5 W. Here, for this particular PT5, the input power was limited by the tunnel junction peak current capability. Based on our other manufacturing data and from alternative TJ designs tested at low temperatures, we expect future PT5 runs will have input power capabilities about an order of magnitude higher.

Remarkably, for example for the 372 mW curve of Figure 2a, the open-circuit voltage (V_{oc}) reaches a value of V_{oc} = 7.184 V, while the maximum power point voltage (V_{mpp}) is then 6.875 V. It corresponds to an average voltage of 1.437 V per subcell, yielding a bandgap

voltage offset value of W_{oc} = 0.071 V, where $W_{oc} = (Eg/q) - V_{oc}$ with Eg being the bandgap energy (here, 1.508 eV for GaAs at 77 K) and q is the electronic charge. The W_{oc} values obtained with the PT5 at low temperatures are therefore significantly better than the best values obtained at room temperature for GaAs with W_{oc} (20 °C) = 0.181 V [41], and also for the long wavelength PT10-InGaAs/InP OPCs with W_{oc} (20 °C) = 0.187 V [47].

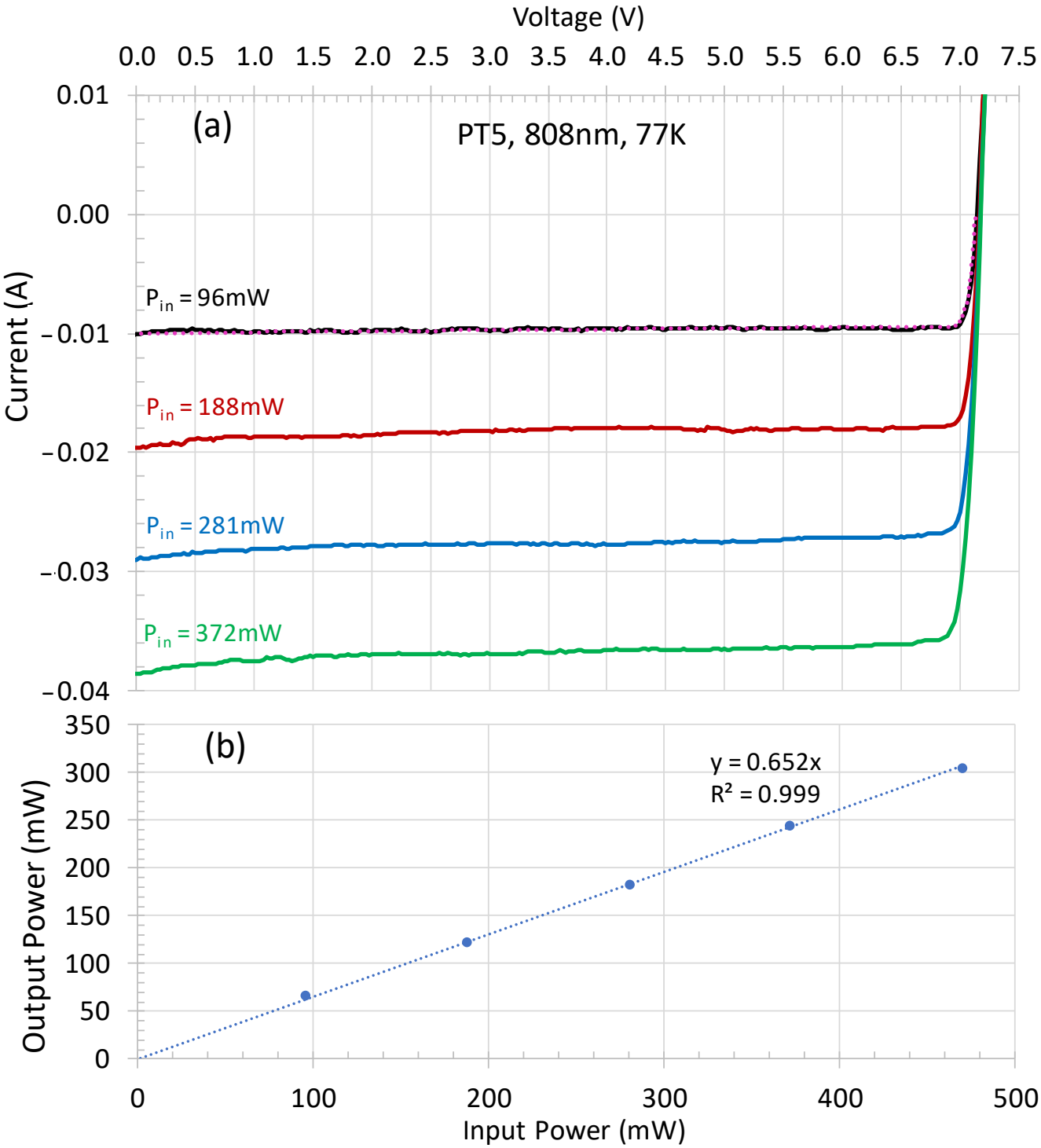

Figure 2. I-V characteristic measured at 77 K for a PT5 OPC illuminated at 808 nm with different input powers (P_{in}) in (**a**), and the resulting output power vs input power relationship in (**b**). The 96 mW data (black curve) in (**a**) is also fitted with a 5J ideal diode model (pink dashed line).

The ideal diode model of Figure 2a can also be used to further explore better optimized, but realistic, conditions: a conversion efficiency of Eff ~ 75% would require improving the EQE to ~87%, while keeping W_{oc} and the diode ideality factors the same. An EQE of 93% would yield an Eff ~80% at 77 K. Such EQE improvements will most likely be achieved by further reducing the mismatch in the subcell's photocurrents. Increasing the optical input intensities in the tens of W/cm^2 could also help to increase the efficiency if the W_{oc} value can be further reduced under higher optical intensities.

The temperature dependence of the PT5 properties are analyzed in more details in Figure 3. The output voltage is shown in Figure 3a for a 1 cm^2 chip mounted into a cryostat equipped with a 1 kOhm RTD and used to directly assess the OPC's temperature while the device is warming up from liquid nitrogen temperature to room temperature. The open-circuit voltage (V_{oc}) is decreased only by few millivolts between liquid nitrogen temperature and about 145 K. The V_{oc} of this larger chip is lower than the V_{oc} obtained for the smaller chip of Figure 2, predominantly because of the relatively low optical intensity used for Figure 3a. More importantly, for the range between 175 K and up to above room temperature, the V_{oc} varies linearly with temperature with a slope of −7 mV/K, as shown from the linear regression in Figure 3a. This temperature coefficient can then be used to calibrate the device temperatures from the measured V_{oc}. For example, Figure 3b shows the measured efficiency as a function of the measured V_{oc} for the PT5 of Figure 2 with an optical input of 100 mW at 808 nm (blue curve). The PT5 parameters are extracted from the full I-V curves taken while the PT5 is warming up from 77 K to room temperature. The PT5 efficiency clearly increases as the device warms up from 77 K and reaches a maximum value of Eff ~72.4% when the V_{oc} reaches 6.7 V. Similar temperature dependence data, as in Figure 3b, were measured for other optical input powers. Input-power-adjusted V_{oc} temperature coefficients (e.g., Figure 3a) are then used to plot the temperature dependence of the conversion efficiency, as shown in Figure 4 for an optical input power of 100 mW and 193 mW (black curve). A maximum conversion efficiency of Eff = 74.7% is here measured for this PT5 at a temperature of about 150 K at P_{in} = 193 mW.

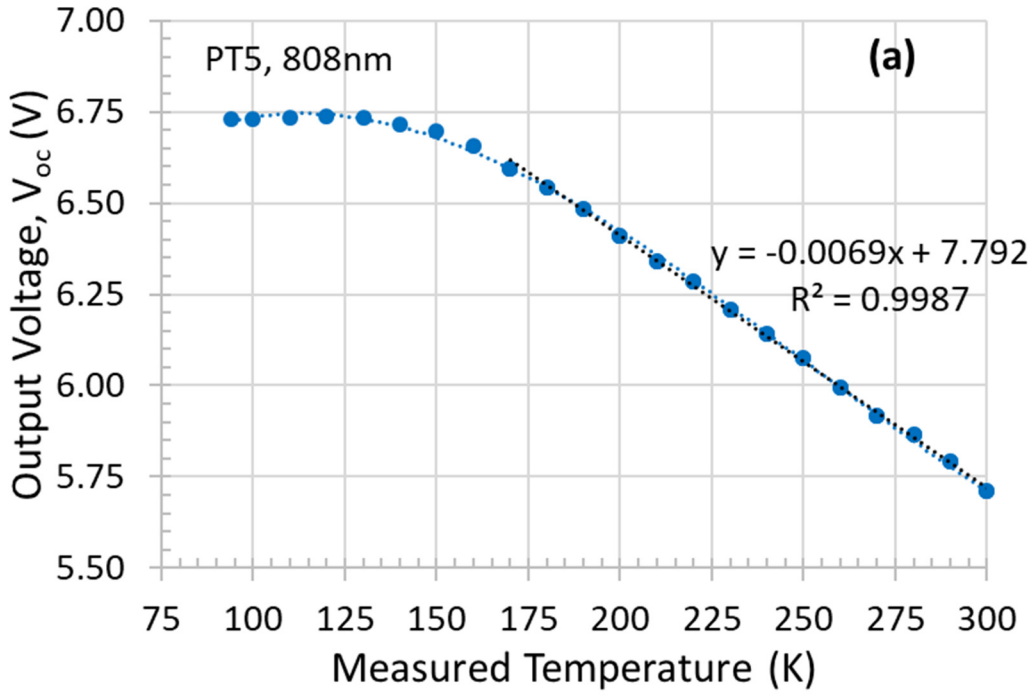

Figure 3. *Cont.*

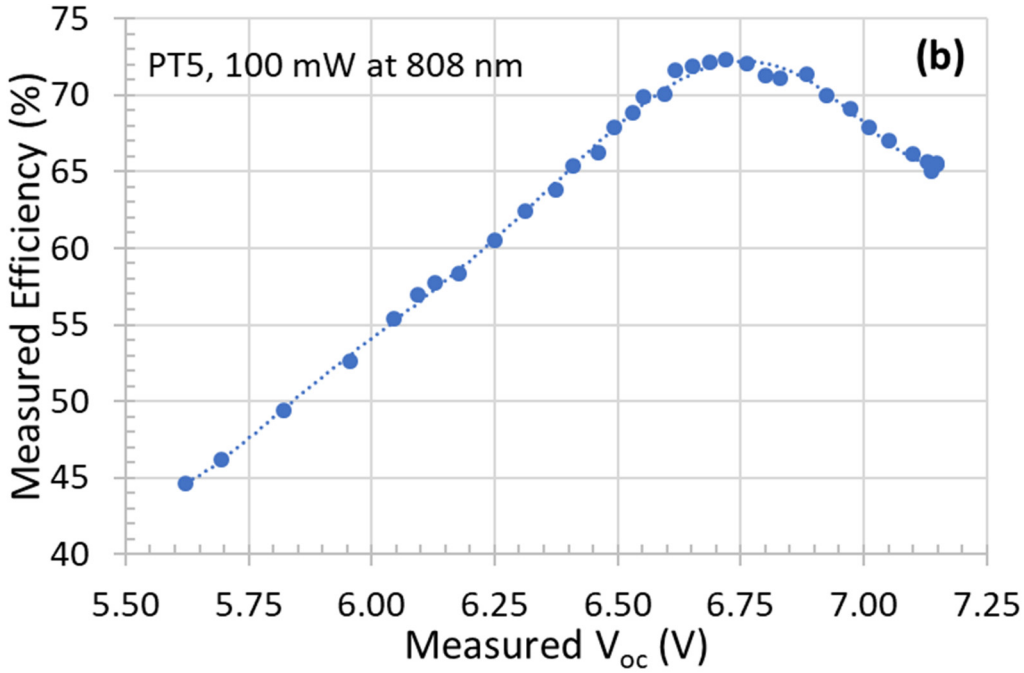

Figure 3. Measured V_{oc} as a function of the temperature in (**a**), and measured conversion efficiency as a function of the measured V_{oc} in (**b**) for a PT5 with an optical input at 808 nm.

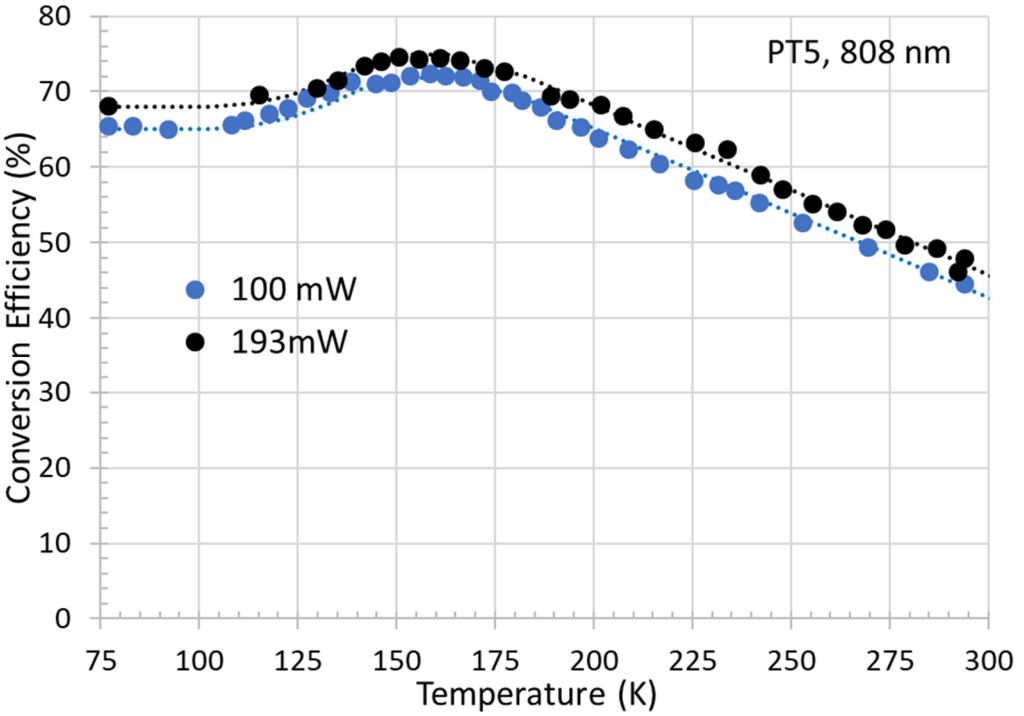

Figure 4. Conversion efficiency as a function of the temperature for the PT5 device with an optical input at 808 nm at 100 mW and 193 mW of input power.

Applying again the ideal diode model to the 150 K I-V curves, we evaluate that for an optical input intensity of ~62 W/cm^2, such PT5 would be expected to have a W_{oc} value of 57 mV and an efficiency of Eff ~ 77.7% (from the diode model, not shown). The latter evaluation is therefore based on the experimental results at lower optical input combined with the diode model projected at higher optical intensities. We expect future runs will achieve these conditions.

4. Discussion

The highest output voltage values are measured at the lowest temperatures. This is expected from the temperature dependence of the bandgap. However, as shown in in Figure 4, the conversion efficiency of the PT5 peaks at intermediate temperatures. Record efficiencies of Eff > 70% are obtained for temperatures between about 130 K and 180 K. This optimum in performance is obtained because the best current matching conditions, for this specific layer design, are realized for that temperature range. For example, Figure 5 shows the temperature dependence of the output voltage in Figure 5a, of the external quantum efficiency measured at the maximum power point (EQE at mpp) in Figure 5b, and of the measured bandgap offset (W_{oc}) in Figure 5c.

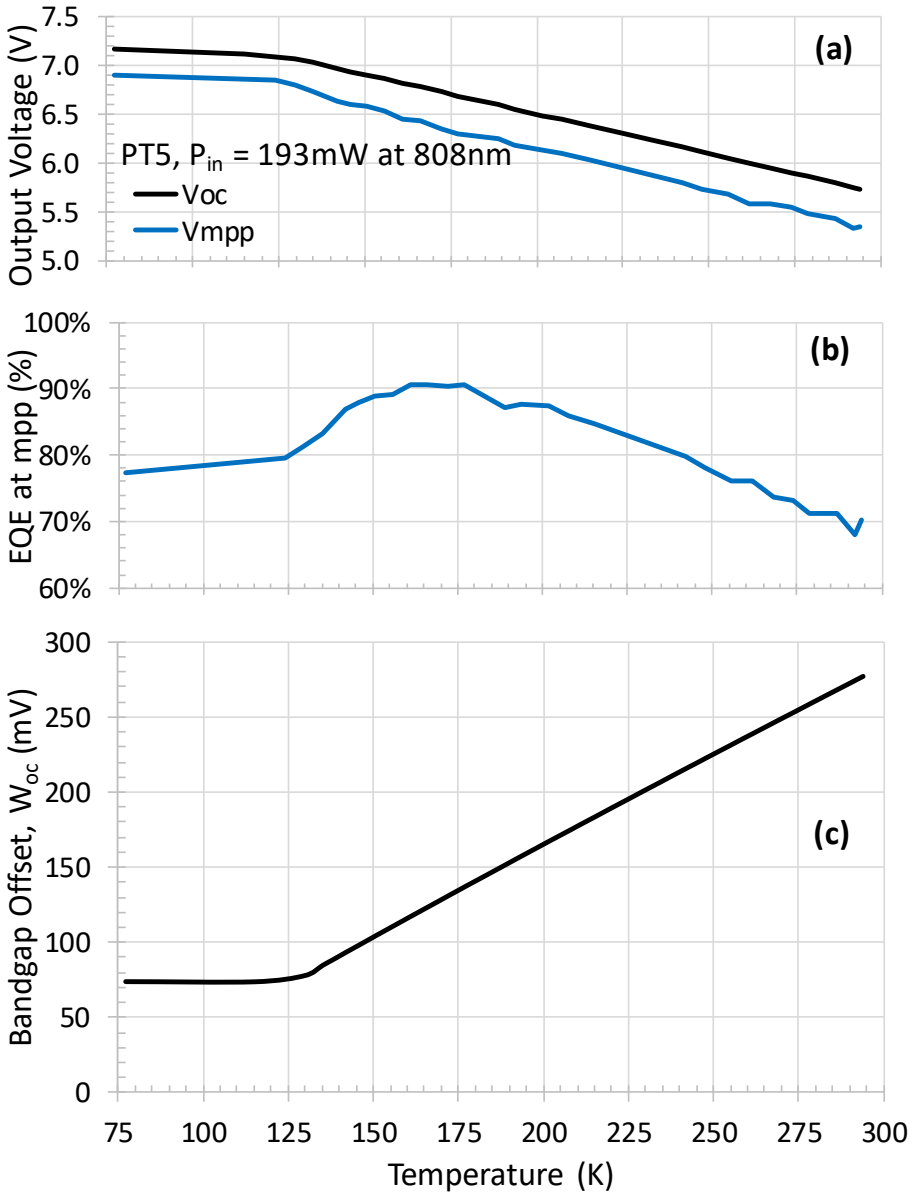

Figure 5. Temperature dependence of the output voltage in (**a**), the external quantum efficiency (EQE at mpp) in (**b**), and the bandgap offset (W_{oc}) in (**c**).

As can be observed in Figure 5b, at an input wavelength of 808 nm, a good current matching condition is indeed obtained in the range of 150 K < T < 180 K, with EQE values of about 90% at the maximum power point. Further incremental improvements could be obtained by insuring a better current matching in all the subcells simultaneously,

minimizing the device reflectivity, and minimizing the gridline shadowing. At lower temperatures the EQE decreases to ~79%, as was also deduced from the ideal diode model of Figure 2a. The EQE also decreases at higher temperatures, reaching about 70% at room temperature, because this particular PT5 was design for an optical input around 850 nm at 20 °C. It can therefore be deduced that at 808 nm at the warmer temperatures, the upper subcells are somewhat overdriven and the bottom subcells are current-starved. Conversely, near 77 K, the upper subcells would be generating less photocurrent relative to the lower subcells.

The V_{oc} data of Figure 5a is used, with the GaAs energy gap calculated using the Varshni equation [86], to extract W_{oc} in Figure 5c. W_{oc} increases linearly above 130 K with a slope of 1.2 mV/K for each individual subcells. This can be explained by the shift of the Fermi levels in the n-type and p-type side of each p/n junction with temperature. An estimate suggests this change should be ~0.3 mV/K for each GaAs junction. For temperatures below 130 K, record W_{oc} values in the range of 75 mV are obtained with negligible temperature dependence. The flatter temperature dependence of W_{oc} below 130K may be caused by changes in the density of states of GaAs affecting the Fermi levels and also from current mismatch in the individual cells affecting slightly the measured V_{oc}. In previous temperature studies of GaAs solar cells [87–91], Philipps et al. have attributed the decrease of the open-circuit voltage with increasing temperature to the temperature dependence of the effective density of states, the charge carrier densities and the band parameter of GaAs [87].

5. Conclusions

In conclusion, record efficiencies have been demonstrated at cryogenic temperatures with the vertical multijunction VEHSA optical power converter. Conversion efficiencies of Eff ~75% have been measured for an input wavelength of 808 nm with the PT5 OPCs. For the specific PT5 design studied, the maximum power point EQE values are reaching ~90% for an optimal temperature range of 150 K < T < 180 K. Record bandgap offset values (W_{oc}) have been obtained, with W_{oc} as low as 71 mV for temperatures below 130 K. The measured data and the corresponding ideal diode multijunction model suggest that multijunction GaAs OPCs for cryogenic operation with conversion efficiencies in the range of 75% to 80% are expected to be realistic with further optimization. The study confirms that OPC devices designed for high performance at cryogenic temperature with an optical input at 808nm should be expected to also operate at high conversion efficiencies at, or near, room temperature using an optical input at 850 nm. These results are expected to be of benefit for a number of experiments requiring electrical isolation under cryogenic conditions, for example conducted in liquid argon [79,92].

Author Contributions: Conceptualization, S.F. and D.P.M.; methodology, S.F. and D.P.M.; software, S.F. and D.P.M.; validation, S.F. and D.P.M.; formal analysis, S.F. and D.P.M.; investigation, S.F. and D.P.M.; data curation, S.F. and D.P.M.; writing—original draft preparation S.F.; writing—review and editing S.F. and D.P.M.; visualization, S.F.; project administration, S.F. and D.P.M.; funding acquisition, S.F. and D.P.M. All authors have read and agreed to the published version of the manuscript.

Funding: This research received no external funding.

Data Availability Statement: The data that support the findings of this study are available from the corresponding author upon reasonable request.

Conflicts of Interest: The authors declare no particular conflict of interest, but it should be noted that the authors are employed by Broadcom, a company that manufactures and sells semiconductor components, including power converter devices.

References

1. Jomen, R.; Tanaka, F.; Akiba, T.; Ikeda, M.; Kiryu, K.; Matsushita, M.; Maenaka, H.; Dai, P.; Lu, S.; Uchida, S. Conversion efficiencies of single-junction III–V solar cells based on InGaP, GaAs, InGaAsP, and InGaAs for laser wireless power transmission. *Jpn. J. Appl. Phys.* **2018**, *57*, 08RD12. [CrossRef]
2. Komuro, Y.; Honda, S.; Kurooka, K.; Warigaya, R.; Tanaka, F.; Uchida, S. A 43.0% efficient GaInP photonic power converter with a distributed Bragg reflector under high-power 638 nm laser irradiation of 17 Wcm^{-2}. *Appl. Phys. Express* **2021**, *14*, 052002. [CrossRef]
3. Schubert, J.; Oliva, E.; Dimroth, F.; Guter, W.; Loeckenhoff, R.; Bett, A.W. High-voltage GaAs photovoltaic laser power converters. *IEEE Trans. Electron Devices* **2009**, *56*, 170–175. [CrossRef]
4. Zhao, Y.; Sun, Y.; He, Y.; Yu, S.; Dong, J. Design and fabrication of six-volt vertically-stacked GaAs photovoltaic power converter. *Sci. Rep.* **2016**, *6*, 38044. [CrossRef] [PubMed]
5. Sun, Y.-R.; Dong, J.-R.; He, Y.; Zhao, Y.-M.; Yu, S.-Z.; Xue, J.-P.; Xue, C.; Wang, J.; Lu, Y.Q.; Ding, Y.-W. A six-junction GaAs laser power converter with different sizes of active aperture. *Optoelectron. Lett.* **2017**, *13*, 21–24. [CrossRef]
6. Yin, J.; Sun, Y.; Yu, S.; Zhao, Y.; Li, R.; Dong, J. 1064 nm InGaAsP multi-junction laser power converters. *J. Semicond.* **2020**, *41*, 062303. [CrossRef]
7. Huang, J.; Sun, Y.; Zhao, Y.; Yu, S.; Dong, J.; Xue, J.; Xue, C.; Xue, C.; Wang, J.; Lu, Y.; et al. Four-junction AlGaAs/GaAs laser power converter. *J. Semicond.* **2018**, *39*, 044003. [CrossRef]
8. Helmers, H.; Lopez, E.; Höhn, O.; Lackner, D.; Schön, J.; Schauerte, M.; Schachtner, M.; Dimroth, F.; Bett, A.W. 68.9% Efficient GaAs-Based Photonic Power Conversion Enabled by Photon Recycling and Optical Resonance. *Phys. Status Solidi (RRL)–Rapid Res. Lett.* **2021**, *15*, 2100113. [CrossRef]
9. Oliva, E.; Dimroth, F.; Bett, A.W. GaAs converters for high power densities of laser illumination. *Prog. Photovolt. Res. Appl.* **2008**, *16*, 289–295. [CrossRef]
10. Mukherjee, J.; Jarvis, S.; Perren, M.; Sweeney, S.J. Efficiency limits of laser power converters for optical power transfer applications. *J. Phys. D Appl. Phys.* **2013**, *46*, 264006. [CrossRef]
11. Fafard, S.; York, M.C.A.; Proulx, F.; Valdivia, C.E.; Wilkins, M.M.; Arès, R.; Aimez, V.; Hinzer, K.; Masson, D.P. Ultrahigh efficiencies in vertical epitaxial heterostructure architectures. *Appl. Phys. Lett.* **2016**, *108*, 071101. [CrossRef]
12. Fafard, S.; Proulx, F.; York, M.C.A.; Richard, L.S.; Provost, P.O.; Arès, R.; Aimez, V.; Masson, D.P. High-photovoltage GaAs vertical epitaxial monolithic heterostructures with 20 thin p/n junctions and a conversion efficiency of 60%. *Appl. Phys. Lett.* **2016**, *109*, 131107. [CrossRef]
13. Khvostikov, V.P.; Kalyuzhnyy, N.A.; Mintairov, S.A.; Sorokina, S.V.; Potapovich, N.S.; Emelyanov, V.M.; Timoshina, N.K.; Andreev, V.M. Photovoltaic laser-power converter based on AlGaAs/GaAs heterostructures. *Semiconductors* **2016**, *50*, 1220–1224. [CrossRef]
14. Olsen, L.C.; Huber, D.A.; Dunham, G.; Addis, F.W. High efficiency monochromatic GaAs solar cells. In Proceedings of the Conference Record of the IEEE Photovoltaic Specialists Conference, Las Vegas, NV, USA, 7–11 October 1991; IEEE: Piscataway, NJ, USA, 1992; Volume 1, pp. 419–424.
15. Krut, D.; Sudharsanan, R.; Isshiki, T.; King, R.; Karam, N.H. A 53% high efficiency GaAs vertically integrated multi-junction laser power converter. In Proceedings of the 65th DRC Device Research Conference, South Bend, IN, USA, 18–20 June 2007; pp. 123–124.
16. Andreev, V.; Khvostikov, V.; Kalinovsky, V.; Lantratov, V.; Grilikhes, V.; Rumyantsev, V.; Shvarts, M.; Fokanov, V.; Pavlov, A. High current density GaAs and GaSb photovoltaic cells for laser power beaming. In Proceedings of the 3rd World Conference on Photovoltaic Energy Conversion, Osaka, Japan, 11–18 May 2003; Volume 1, pp. 761–764.
17. Peña, R.; Algora, C.; Anton, I. GaAs multiple photovoltaic converters with an efficiency of 45% for monochromatic illumination. In Proceedings of the 3rd World Conference on Photovoltaic Energy Conversion, Osaka, Japan, 11–18 May 2003; Volume 1, pp. 228–231.
18. Kalyuzhnyy, N.A.; Emelyanov, V.M.; Mintairov, S.A.; Shvarts, M.Z. InGaAs metamorphic laser (λ=1064 nm) power converters with over 44% efficiency. In *AIP Conference Proceedings*; AIP Publishing LLC: Melville, NY, USA, 2018; Volume 2012, p. 110002.
19. Kim, Y.; Shin, H.B.; Lee, W.H.; Jung, S.H.; Kim, C.Z.; Kim, H.; Lee, Y.T.; Kang, H.K. 1080 nm InGaAs laser power converters grown by MOCVD using InAlGaAs metamorphic buffer layers. *Sol. Energy Mater. Sol. Cells* **2019**, *200*, 109984. [CrossRef]
20. Law, H.D.; Ng, W.W.; Nakano, K.; Dapkus, P.D.; Stone, D.R. High Efficiency InGaAsP Photovoltaic Power Converter. *IEEE Electron Device Lett.* **1981**, *2*, 26–27. [CrossRef]
21. Panchak, A.N.; Pokrovskiy, P.V.; Malevskiy, D.A.; Larionov, V.R.; Shvarts, M.Z. High-Efficiency Conversion of High-Power-Density Laser Radiation. *Tech. Phys. Lett.* **2019**, *45*, 24–26. [CrossRef]
22. Bett, A.W.; Dimroth, F.; Lockenhoff, R.; Oliva, E.; Schubert, J. III–V solar cells under monochromatic illumination. In Proceedings of the Conference Record of the IEEE Photovoltaic Specialists Conference, San Diego, CA, USA, 11–16 May 2008.
23. Fahrenbruch, A.L.; Lopez-Otero, L.; Werthern, J.G.; Wu, T.C. GaAs- and InAlGaAs-based concentrator-type cells for conversion of power transmitted by optical fibers. In Proceedings of the Conference Record of the IEEE Photovoltaic Specialists Conference, Washington, DC, USA, 13–17 May 1996; pp. 117–120.
24. Fave, A.; Kaminski, A.; Gavand, M.; Mayet, L.; Laugier, A. GaAs converter for high power laser diode. In Proceedings of the Conference Record of the IEEE Photovoltaic Specialists Conference, Washington, DC, USA, 13–17 May 1996; pp. 101–104.

25. Green, M.A.; Zhao, J.; Wang, A.; Wenham, S.R. 45% Efficient Silicon Photovoltaic Cell Under Monochromatic Light. *IEEE Electron Device Lett.* **1992**, *13*, 317–318. [CrossRef]
26. Höhn, O.; Walker, A.W.; Bett, A.W.; Helmers, H. Optimal laser wavelength for efficient laser power converter operation over temperature. *Appl. Phys. Lett.* **2016**, *108*, 241104. [CrossRef]
27. Shan, T.; Qi, X. Design and optimization of GaAs photovoltaic converter for laser power beaming. *Infrared Phys. Technol.* **2015**, *71*, 144–150. [CrossRef]
28. Khvostikov, V.P.; Sorokina, S.V.; Potapovich, N.S.; Khvostikova, O.A.; Timoshina, N.K.; Shvarts, M.Z. Modification of Photovoltaic Laser-Power (λ = 808 nm) Converters Grown by LPE. *Semiconductors* **2018**, *52*, 366–370. [CrossRef]
29. Khvostikov, V.P.; Sorokina, S.V.; Potapovich, N.S.; Khvostikova, O.A.; Timoshina, N.K. Laser (λ = 809 nm) power converter based on GaAs. *Semiconductors* **2017**, *51*, 645. [CrossRef]
30. Helmers, H.; Franke, A.; Lackner, D.; Höhn, O.; Predan, F.; Dimroth, F. 51% Efficient Photonic Power Converters for O-Band Wavelengths around 1310 nm. In Proceedings of the Conference Record of the IEEE Photovoltaic Specialists Conference, Calgary, AB, Canada, 15 June–21 August 2020; pp. 2471–2474.
31. Zhao, Y.; Liang, P.; Ren, H.; Han, P. Enhanced efficiency in 808 nm GaAs laser power converters via gradient doping. *AIP Adv.* **2019**, *9*, 105206. [CrossRef]
32. York, M.C.A.; Fafard, S. High efficiency phototransducers based on a novel vertical epitaxial heterostructure architecture (VEHSA) with thin p/n junctions. *J. Phys. D Appl. Phys.* **2017**, *50*, 173003. [CrossRef]
33. Huang, J.; Sun, Y.; Zhao, Y.; Yu, S.; Li, K.; Dong, J.; Xue, J.; Xue, C.; Ye, Y. Characterizations of high-voltage vertically-stacked GaAs laser power converter. *J. Semicond.* **2018**, *39*, 094006. [CrossRef]
34. Ding, Y.; Li, Q.; Lu, Y.; Wang, J. TO-packaged, multi-junction GaAs laser power converter with output electric power over 1 W. In Proceedings of the Conference on Lasers and Electro-Optics Pacific Rim (CLEO-PR), Singapore, 31 July–4 August 2017; pp. 1–3.
35. Jarvis, S.D.; Mukherjee, J.; Perren, M.; Sweeney, S.J. Development and characterisation of laser power converters for optical power transfer applications. *IET Optoelectron.* **2014**, *8*, 64–70. [CrossRef]
36. Khvostikov, V.P.; Sorokina, S.V.; Khvostikova, O.A.; Potapovich, N.S.; Malevskaya, A.V.; Nakhimovich, M.V.; Shvarts, M.Z. GaSb photovoltaic cells for laser power conversion. In *AIP Conference Proceedings*; AIP Publishing LLC: Melville, NY, USA, 2019; Volume 2149, p. 050007.
37. Fafard, S.; Masson, D.; Werthen, J.G.; Liu, J.; Wu, T.C.; Hundsberger, C.; Schwarzfischer, M.; Steinle, G.; Gaertner, C.; Piemonte, C.; et al. Power and Spectral Range Characteristics for Optical Power Converters. *Energies* **2021**, *14*, 4395. [CrossRef]
38. Keller, G. GaAs multi-junction laser power converters at AZUR SPACE: Current status and development activities. In Proceedings of the 1st Optical Wireless Fiber Power Transmiss. Conference, Yokohama, Japan, 23–25 April 2019; pp. 11–12.
39. Wojtczuk, S.J. Long-wavelength laser power converters for optical fibers. In Proceedings of the Conference Record of the Twenty Sixth IEEE Photovoltaic Specialists Conference, Anaheim, CA, USA, 9 September–3 October 1997; pp. 971–974.
40. Eggert, N.; Rusack, R.; Mans, J. Evaluation of photonic power converters. *J. Instrum.* **2010**, *5*, T02001. [CrossRef]
41. Fafard, S.; Masson, D.P. Perspective on photovoltaic optical power converters. *J. Appl. Phys.* **2021**, *130*, 160901. [CrossRef]
42. Wang, A.C.; Sun, Y.R.; Yu, S.Z.; Yin, J.J.; Zhang, W.; Wang, J.S.; Fu, Q.X.; Han, Y.H.; Qin, J.; Dong, J.R. Characteristics of 1520 nm InGaAs multijunction laser power converters. *Appl. Phys. Lett.* **2021**, *119*, 243902. [CrossRef]
43. Kurooka, K.; Honda, T.; Komazawa, Y.; Warigaya, R.; Uchida, S. 46.7% efficient GaInP photonic power converter under high-power 638 nm laser uniform irradiation of 1.5 W cm^{-2}. *Appl. Phys. Express* **2022**, *15*, 062003. [CrossRef]
44. Helmers, H.; Hohn, O.; Tibbits, T.; Schauerte, M.; Amin, H.M.N.; Lackner, D. Unlocking 1550 nm laser power conversion by InGaAs single- and multiple-junction PV cells. In Proceedings of the PVSC 2022- IEEE 49th Photovoltaic Specialists Conference, Philadelphia, PA, USA, 5–10 June 2022.
45. Fafard, S.; York, M.C.A.; Proulx, F.; Wilkins, M.; Valdivia, C.E.; Bajcsy, M.; Ban, D.; Arès, R.; Aimez, V.; Hinzer, K.; et al. Ultra-efficient N-junction photovoltaic cells with V_{oc} > 14 V at high optical input powers. In Proceedings of the PVSC 2016-IEEE 43rd Photovoltaic Specialists Conference, Portland, OR, USA, 5–10 June 2016; p. 2374.
46. Fafard, S.; Masson, D.; Werthen, J.-G.; Liu, J.; Wu, T.C.; Hundsberger, C.; Schwarzfischer, M.; Steinle, G.; Gaertner, C.; Piemonte, C.; et al. High performance laser power converters and applications. In Proceedings of the Technical Digest of the 4th Optical Wireless and Fiber Power Trans. Conference (OWPT2022), Yokohama, Japan, 18–21 April 2022.
47. Fafard, S.; Masson, D.P. High-Efficiency and High-Power Multijunction InGaAs/InP Photovoltaic Laser Power Converters for 1470 nm. *Photonics* **2022**, *9*, 438. [CrossRef]
48. Lozano, J.F.; Seoane, N.; Comesaña, E.; Almonacid, F.; Fernández, E.F.; García-Loureiro, A. Laser Power Converter Architectures Based on 3C-SiC with Efficiencies >80%. *Sol. RRL* **2022**, *6*, 2101077. [CrossRef]
49. Fernández, E.F.; García-Loureiro, A.; Seoane, N.; Almonacid, F. Band-gap material selection for remote high-power laser transmission. *Sol. Energy Mater. Sol. Cells* **2022**, *235*, 111483. [CrossRef]
50. France, R.M.; Buencuerpo, J.; Bradsby, M.; Geisz, J.F.; Sun, Y.; Dhingra, P.; Lee, M.L.; Steiner, M.A. Graded buffer Bragg reflectors with high reflectivity and transparency for metamorphic optoelectronics. *J. Appl. Phys.* **2021**, *129*, 173102. [CrossRef]
51. Beattie, M.N.; Valdivia, C.E.; Wilkins, M.M.; Zamiri, M.; Kaller, K.L.C.; Tam, M.C.; Kim, H.S.; Krich, J.J.; Wasilewski, Z.R.; Hinzer, K. High current density tunnel diodes for multi-junction photovoltaic devices on InP substrates. *Appl. Phys. Lett.* **2021**, *118*, 062101. [CrossRef]

52. Wagner, L.; Reichmuth, S.K.; Philipps, S.P.; Oliva, E.; Bett, A.W.; Helmers, H. Integrated series/parallel connection for photovoltaic laser power converters with optimized current matching. *Prog. Photovolt. Res. Appl.* **2020**, *29*, 172–180. [CrossRef]
53. Panchak, A.; Khvostikov, V.; Pokrovskiy, P. AlGaAs gradient waveguides for vertical p/n junction GaAs laser power con-verters. *Opt. Laser Technol.* **2021**, *136*, 106735. [CrossRef]
54. Lin, M.; Sha, W.E.; Zhong, W.; Xu, D. Intrinsic losses in photovoltaic laser power converters. *Appl. Phys. Lett.* **2021**, *118*, 104103. [CrossRef]
55. Zhao, Y.; Li, S.; Ren, H.; Li, S.; Han, P. Energy band adjustment of 808 nm GaAs laser power converters via gradient doping. *J. Semicond.* **2021**, *42*, 032701. [CrossRef]
56. Nouri, N.; Valdivia, C.E.; Beattie, M.N.; Zamiri, M.S.; Krich, J.J.; Hinzer, K. Ultrathin monochromatic photonic power converters with nanostructured back mirror for light trapping of 1310-nm laser illumination. In *Physics, Simulation, and Photonic Engineering of Photovoltaic Devices X*; SPIE: Bellingham, WA, USA, 2021; Volume 11681, p. 116810X.
57. Masson, D.; Proulx, F.; Fafard, S. Pushing the limits of concentrated photovoltaic solar cell tunnel junctions in novel high-efficiency GaAs phototransducers based on a vertical epitaxial heterostructure architecture. *Prog. Photovolt. Res. Appl.* **2015**, *23*, 1687–1696. [CrossRef]
58. Fafard, S.; Masson, D.P. Transducer to Convert Optical Energy to Electrical Energy. US Patent 9,673,343, 6 June 2017.
59. Wulf, J.; Oliva, E.; Mikolasch, G.; Bartsch, J.; Dimroth, F.; Helmers, H. Thin film GaAs solar cell enabled by direct rear side plating and patterned epitaxial lift-off. In Proceedings of the 2021 IEEE 48th Photovoltaic Specialists Conference (PVSC), Fort Lauderdale, FL, USA, 20–25 June 2021; p. 1931.
60. Helmers, H.; Lopez, E.; Höhn, O.; Lackner, D.; Schön, J.; Schauerte, M.; Schachtner, M.; Dimroth, F.; Bett, A.W. Pushing the Boundaries of Photovoltaic Light to Electricity Conversion: A GaAs Based Photonic Power Converter with 68.9% Efficiency. In Proceedings of the 2021 IEEE 48th Photovoltaic Specialists Conference (PVSC), Fort Lauderdale, FL, USA, 20–25 June 2021; pp. 2286–2289.
61. Schauerte, M.; Höhn, O.; Wierzkowski, T.; Keller, G.; Helmers, H. 4-Junction GaAs Based Thin Film Photonic Power Converter with Back Surface Reflector for Medical Applications. In Proceedings of the 2021 IEEE 48th Photovoltaic Specialists Conference (PVSC), Fort Lauderdale, FL, USA, 20–25 June 2021; pp. 1954–1959.
62. France, R.M.; Hinojosa, M.; Ahrenkiel, S.P.; Young, M.R.; Johnston, S.W.; Guthrey, H.L.; Steiner, M.A.; Geisz, J.F. Improvement of front-junction GaInP by point-defect injection and annealing. In Proceedings of the 2021 IEEE 48th Photovoltaic Specialists Conference (PVSC), Fort Lauderdale, FL, USA, 20–25 June 2021; p. 2522.
63. Geisz, J.F.; Buencuerpo, J.; McMahon, W.E.; Klein, T.R.; Tamboli, A.C.; Warren, E.L. Fabrication, Measurement, and Modeling of GaInP/GaAs Three-Terminal Cells and Strings. In Proceedings of the 2021 IEEE 48th Photovoltaic Specialists Conference (PVSC), Fort Lauderdale, FL, USA, 20–25 June 2021; pp. 0154–0157.
64. Yamaguchi, M.; Dimroth, F.; Geisz, J.F.; Ekins-Daukes, N.J. Multi-junction solar cells paving the way for super high-efficiency. *J. Appl. Phys.* **2021**, *129*, 240901. [CrossRef]
65. Kimovec, R.; Helmers, H.; Bett, A.W.; Topič, M. Comprehensive electrical loss analysis of monolithic interconnected multi-segment laser power converters. *Prog. Photovolt. Res. Appl.* **2019**, *27*, 199–209. [CrossRef]
66. Helmers, H.; Bett, A.W.; Topič, M. On the Influence of the Photo-Induced Leakage Current in Monolithically Interconnected Modules. *IEEE J. Photovolt.* **2018**, *8*, 541–546.
67. Čičić, S.; Tomić, S. Automated design of multi junction solar cells by genetic approach: Reaching the> 50% efficiency target. *Sol. Energy Mater. Sol. Cells* **2018**, *181*, 30–37. [CrossRef]
68. Algora, C.; García, I.; Delgado, M.; Peña, R.; Vázquez, C.; Hinojosa, M.; Rey-Stolle, I. Beaming power: Photovoltaic laser power converters for power-by-light. *Joule* **2022**, *6*, 340. [CrossRef]
69. Matsuura, M.; Nomoto, H.; Mamiya, H.; Higuchi, T.; Masson, D.; Fafard, S. Over 40-W Electric Power and Optical Data Transmission Using an Optical Fiber. *IEEE Trans. Power Electron.* **2020**, *36*, 4532. [CrossRef]
70. Helmers, H.; Armbruster, C.; von Ravenstein, M.; Derix, D.; Schöner, C. 6-W Optical Power Link With Integrated Optical Data Transmission. *IEEE Trans. Power Electron.* **2020**, *35*, 7904. [CrossRef]
71. Jaffe, P. Practical Power Beaming Gets Real. IEEE Spectrum. 21 May 2022. Available online: https://spectrum.ieee.org/power-beaming (accessed on 15 June 2022).
72. Wilkins, M.M.; Ishigaki, M.; Provost, P.O.; Masson, D.; Fafard, S.; Valdivia, C.E.; Dede, E.M.; Hinzer, K. Ripple-free boost-mode power supply using photonic power conversion. *IEEE Trans. Power Electron.* **2018**, *34*, 1054–1064. [CrossRef]
73. Sweeney, S.J. Optical wireless power at eye-safe wavelengths: Challenges and opportunities. In Proceedings of the 3rd Optical Wireless and Fiber Power Transmission Conference (OWPT2021), Yokohama, Japan, 19–22 April 2021.
74. Wong, Y.L.; Shibui, S.; Koga, M.; Hayashi, S.; Uchida, S. Optical Wireless Power Transmission Using a GaInP Power Converter Cell under High-Power 635 nm Laser Irradiation of 53.5 W/cm^2. *Energies* **2022**, *15*, 3690. [CrossRef]
75. Kalyuzhnyy, N.A.; Emelyanov, V.M.; Evstropov, V.V.; Mintairov, S.A.; Mintairov, M.A.; Nahimovich, M.V.; Salii, R.A.; Shvarts, M.Z. Optimization of photoelectric parameters of InGaAs metamorphic laser (λ = 1064 nm) power converters with over 50% efficiency. *Sol. Energy Mater. Sol. Cells* **2020**, *217*, 110710. [CrossRef]
76. He, T.; Yang, S.H.; Zhang, H.Y.; Zhao, C.M.; Zhang, Y.C.; Xu, P.; Muñoz, M.Á. High-power high-efficiency laser power transmission at 100 m using optimized multi-cell GaAs converter. *Chin. Phys. Lett.* **2014**, *31*, 104203. [CrossRef]

77. Khvostikov, V.P.; Kalyuzhnyy, N.A.; Mintairov, S.A.; Potapovich, N.S.; Sorokina, S.V.; Shvarts, M.Z. Module of Laser-Radiation (λ = 1064 nm) Photovoltaic Converters. *Semiconductors* **2019**, *53*, 1110–1113. [CrossRef]
78. Li, L.; Ji, H.-M.; Luo, S.; Xu, P.; Gao, Q.; Lv, H.; Liu, W. Fabrication and Characterization of a High-Power Assembly With a 20-Junction Monolithically Stacked Laser Power Converter. *IEEE J. Photovolt.* **2018**, *8*, 1355–1362.
79. Delgado, M.; Gutiérrez, R.M.; Fuentes, F. Liquid argon photodetection systems for neutrino detectors: A minireview. *J. Phys. Conf. Ser.* **2020**, *1672*, 012009. [CrossRef]
80. Čičić, S.; Tomić, S. Genetic algorithm designed high efficiency laser power converters based on the vertical epitaxial heterostructure architecture. *Sol. Energy Mater. Sol. Cells* **2019**, *200*, 109878. [CrossRef]
81. Proulx, F.; York, M.C.; Provost, P.O.; Arès, R.; Aimez, V.; Masson, D.P.; Fafard, S. Measurement of strong photon recycling in ultra-thin GaAs n/p junctions monolithically integrated in high-photovoltage vertical epitaxial heterostructure architec-tures with conversion efficiencies exceeding 60%. *Phys. Status Solidi (RRL)* **2017**, *11*, 1600385. [CrossRef]
82. Wilkins, M.; Valdivia, C.E.; Gabr, A.M.; Masson, D.; Fafard, S.; Hinzer, K. Luminescent coupling in planar opto-electronic devices. *J. Appl. Phys.* **2015**, *118*, 143102. [CrossRef]
83. Lopez, E.; Höhn, O.; Schauerte, M.; Lackner, D.; Schachtner, M.; Reichmuth, S.K.; Helmers, H. Experimental coupling process efficiency and benefits of back surface reflectors in photovoltaic multi-junction photonic power converters. *Prog. Photovolt. Res. Appl.* **2021**, *29*, 461–470. [CrossRef]
84. Xia, D.; Krich, J.J. Efficiency increase in multijunction monochromatic photovoltaic devices due to luminescent coupling. *J. Appl. Phys.* **2020**, *128*, 013101. [CrossRef]
85. A BWT Beijing Ltd. Laser Diode Was Used as the 808 nm Source. Available online: https://www.bwt-bj.com/en/product/ (accessed on 20 July 2022).
86. Varshni, Y.P. Temperature dependence of the energy gap in semiconductors. *Physica* **1967**, *34*, 149. [CrossRef]
87. Philipps, S.P.; Hoheisel, R.; Gandy, T.; Stetter, D.; Hermle, M.; Dimroth, F.; Bett, A.W. An experimental and theoretical study on the temperature dependence of GaAs solar cells. In Proceedings of the 2011 37th IEEE Photovoltaic Specialists Conference, Seattle, WA, USA, 19–24 June 2011; pp. 001610–001614.
88. Campesato, R.; Flores, C. Effects of low temperatures and intensities on GaAs and GaAs/Ge solar cells. *IEEE Trans. Electron Devices* **1991**, *38*, 1233–1237. [CrossRef]
89. Aldao, C.M.; Waddill, G.D.; Benning, P.J.; Capasso, C.; Weaver, J.H. Photovoltaic effects in temperature-dependent Fermi-level movement for GaAs(110). *Phys. Rev. B* **1990**, *41*, 6092. [CrossRef] [PubMed]
90. Hoheisel, R.; Walters, R.J.; Bett, A.W. Low temperature effects in photovoltaic devices for deep space missions. In Proceedings of the 2015 IEEE 42nd Photovoltaic Specialist Conference (PVSC), New Orleans, LA, USA, 14–19 June 2015; p. 1.
91. Algora, C.; Ortiz, E.; Rey-Stolle, I.; Díaz, V.; Peña, R.; Andreev, V.M.; Khvostikov, V.P.; Rumyantsev, V.D. A GaAs solar cell with an efficiency of 26.2% at 1000 suns and 25.0% at 2000 suns. *IEEE Trans. Electron Devices* **2001**, *48*, 840. [CrossRef]
92. Abud, A.A.; Abi, B.; Acciarri, R.; Acero, M.A.; Adames, M.R.; Adamov, G.; Adamowski, M.; Adams, D.; Adinolfi, M.; Aduszkiewicz, A.; et al. Scintillation light detection in the 6-m drift-length ProtoDUNE Dual Phase liquid argon TPC. *Eur. Phys. J. C* **2022**, *82*, 618. [CrossRef] [PubMed]